Translational

Molecular Histopathology Using Gold Nanorods and Optical Coherence Tomography

Shradha Prabhulkar,[1] *Jared Matthews,*[2] *Siddarth Rawal,*[3] *and Richard M. Awdeh*[1]

Purpose. To examine the novel application of a commercially available optical coherence tomography (OCT) system toward molecular histopathology using gold nanorod (GNR) linked antibodies as a functionalized contrast agent to evaluate ocular surface squamous neoplasia (OSSN).

Methods. GNRs were synthesized and covalently attached to anti–glucose transporter-1 (GLUT-1) antibodies via carbodiimide chemistry. Three specimens from each of three distinct categories of human conjunctival tissue were selected for analysis, including conjunctiva without epithelial atypia (controls); conjunctival intraepithelial neoplasia, carcinoma in situ (CIS); and conjunctival squamous cell carcinoma (SCC). Tissue sections were incubated initially with GNR tagged anti–GLUT-1 antibodies and then with a fluorescent-tagged secondary antibody. Immunofluorescence and OCT imaging of the tissue was performed and the results were correlated to the light microscopic findings on traditional hemotoxyin and eosin stained sections.

Results. No binding of the functionalized GNRs was observed within the epithelium of three normal conjunctiva controls. While immunofluorescence disclosed variable binding of the functionalized GNRs to atypical epithelial cells in all six cases of OSSN, the enhancement of the OCT signal in three cases of CIS was insufficient to distinguish these specimens from normal controls. In two of three cases of SCC, binding of functionalized GNRs was sufficient to produce an increased scattering effect on OCT in areas correlating to atypical epithelial cells which stained intensely on immunofluorescence imaging. Binding of functionalized GNRs was sufficient to produce an increased scattering effect on OCT in areas correlating to regions of erythrocytes and hemorrhage which stained intensely on immunofluorescence imaging within all nine tested samples.

Conclusions. We have demonstrated the use of OCT for molecular histopathology using functionalized gold nanorods in the setting of OSSN. Our results suggest a threshold concentration of functionalized GNRs within tissue is required to achieve a detectable enhancement in scattering of the OCT signal. (*Invest Ophthalmol Vis Sci.* 2013;54:1192–1200) DOI: 10.1167/iovs.12-10794

Optical coherence tomography (OCT) is a noncontact bioimaging technology that produces high resolution, cross-sectional images of the internal microstructure of tissue by detecting backscattered and backreflected light. OCT relies on low coherence interferometry to measure time delay and intensity of back scattered light.[1] In ophthalmology, OCT enables noninvasive, cross-sectional, in vivo imaging of the retina and anterior eye.[2]

Since the introduction of OCT in 1991, the image quality and axial resolution of the technique has undergone a remarkable evolution, with newer ultra high resolution systems achieving axial resolutions less than 1 μm.[3–5] An active area of investigation is the development of molecular mechanisms for OCT imaging, an approach which has the potential of greatly expanding the diagnostic utility of the technique.[6] The introduction of exogenous contrast agents is one potential means of achieving molecular imaging with OCT; however, as OCT is a coherence imaging technique, it is inherently blind to fluorescent or bioluminescent markers.[7] Much recent work has focused on metallic nanoparticles, particularly gold nanorods (GNRs) as a potential alternative.[8–10]

GNRs have demonstrated the remarkable capacity to absorb and scatter light at visible and near infrared (NIR) regions.[11,12] These optical properties depend on nanoparticles size, shape, and dielectric environment, enabling their application as novel imaging and sensing probes.[13] The principle of using OCT for GNR detection relies on the local surface plasmon resonance effect caused by the incident OCT light.[14] The collective, in phase oscillations of conductive electrons in metallic nanoparticles is known as surface plasmon or particle plasmon resonance. This collective electron oscillation causes considerable local field enhancements at the resonance frequency of the particle plasmon.[15] GNRs are preferred over other shapes of nanoparticles, as their plasmon resonant wavelength can be precisely tuned to the central wavelength of the OCT beam. They have excellent biocompatibility, are nontoxic, and are not susceptible to photo bleaching. GNRs also have very high quality factors and surface areas, which translate to large local field enhancements.[16] Importantly, the surfaces of GNRs can be easily modified to allow for antibody conjugation which enables the use of GNRs as functionalized OCT contrast agents with molecular specificity.[12,17]

The purpose of our study is to demonstrate the use of a commercially available OCT system toward molecular histopathology using antibody-conjugated GNRs as a functionalized contrast agent. We chose to use ocular surface squamous neoplasia (OSSN) as a model to evaluate our technique. To our knowledge, this is the first application of this technique to ocular tissue.

From the [1]Department of Ophthalmology, University of Miami-Bascom Palmer Eye Institute, Miami, Florida; [2]Florida Lions Ocular Pathology Laboratory, Bascom Palmer Eye Institute and the [3]Department of Pathology, University of Miami-Miller School of Medicine, Miami, Florida.

Supported by grants from the National Institutes of Health (R21EY020940 [RMA]), and The Wallace H. Coulter Center for Translational Research (RMA).

Submitted for publication August 17, 2012; revised December 10, 2012; accepted December 25, 2012.

Disclosure: **S. Prabhulkar**, None; **J. Matthews**, None; **S. Rawal**, None; **R.M. Awdeh**, None

Corresponding author: Shradha Prabhulkar, 1501 NW 10th Avenue, BRB Building, Room 742E, Miami, FL 33136; sprabhulkar@med.miami.edu.

Investigative Ophthalmology & Visual Science, February 2013, Vol. 54, No. 2

Utilizing OSSN as a model tissue analyte afforded us a number of advantages. OSSN is an umbrella term encompassing a spectrum from simple dysplasia of the cornea and conjunctival epithelium to carcinoma in situ to invasive squamous cell carcinoma.[18] This allowed us to more thoroughly evaluate the sensitivity of our technique by comparing results across lesions of varying severity. OSSN specimens are also readily available at our institution, likely a consequence of lifestyle and sun exposure. Finally, OSSN lesions have been shown to overexpress anti–glucose transporter-1 (Glut-1), a membrane associated, facilitative glucose transport protein,[19] providing us with a potential molecular target for our functionalized contrast agent. Glut-1 is normally expressed on the cell membrane of erythrocytes and by the endothelial cells of the blood–brain barrier.[20,21] Glut-1 overexpression has been observed in a number of human cancers, including breast, pancreatic, hepatic, esophageal, brain, renal, lung, cutaneous, endometrial, ovarian, and cervical disease.[22–24] The elevation in Glut-1 expression is related to altered metabolic rates and increased glucose consumption of neoplastic cells.[25,26] We were, thus, able to utilize anti–Glut-1 conjugated GNRs as a functionalized OCT contrast agent in the setting of OSSN.

Currently used methods to differentiate between pterygium, carcinoma in situ (CIS), and conjunctival squamous cell carcinoma (SCC) are mainly clinical examination, impression cytologic analysis,[27,28] histopathologic examination, brush cytology,[29] and in vivo confocal microscopy.[30,31] However, these methods have their own limitations related to sensitivity, depth of analysis, need for invasive biopsies that could lead to scarring, and limited field of view of imaging. Prototype high resolution OCT systems have demonstrated the ability to differentiate between CIS and pterygium.[32,33] Using GNRs as targeted contrast agent in synergy with these high resolution OCT systems will allow enhanced diagnostic and monitoring capabilities. The development of contrast agent toward OCT imaging is crucial toward molecular diagnosis and prognosis of ocular disease.

Materials and Methods

Cetyl trimethylammonium bromide (CTAB), chloroauric acid ($HAuCl_4$), sodium borohydride ($NaBH_4$), silver nitrate ($AgNO_3$), ascorbic acid, benzyldimethylammoniumchloride hydrate (BDAC), 11-mercaptodecanoic acid, polyacrylic acid (PAA, molecular weight ~15,000), 3,3′,5,5′ tetramethylbenzidine (TMB), and MES buffer (pH = 6) were purchased from Sigma-Aldrich (St. Louis, MO). SH-PEG-COOH bidirectional polymer was obtained from Nanocs (New York, NY). 1-Ethyl-3-[3-dimethylaminopropyl] carbodiimide (EDC), N-hydroxysulfosuccinimide (NHSS), and rabbit polyclonal antihuman Glut-1 antibody were obtained from Thermo Fisher Scientific Inc. (Rockford, IL). Human Glut-1 protein was purchased from Alpha Diagnostics International Inc. (San Antonio, TX). Horseradish peroxidase labeled antirabbit secondary antibodies were purchased from Abcam (Cambridge, MA). Alexa-488 antirabbit Immunoglobulin G (IgG) (Secondary Antibody) was purchased from Invitrogen Inc. (Carlsbad, CA). Human conjunctival tissue samples were selected from the specimen library of the Florida Lions Ocular Pathology Laboratory at Bascom Palmer Eye Institute as described below.

Preparation of Gold Nanoparticles/Nanoseeds

Two milliliters of 0.20 M CTAB solution was sonicated with 2 mL of 0.5 mM $HAuCl_4$ solution for a period of 10 minutes at a temperature of 40°C until the solution was clear. Once the solution was cooled down to room temperature, 240 μL of 0.01 M ice cold $NaBH_4$ was added to it and stirred for 2 minutes. The final brownish yellow seed solution was stored at 25°C until further use.

Preparation and Characterization of Gold Nanorods

GNRs were synthesized using a two part (CTAB:BDAC) surfactant system. The growth solution consisted of 50 mL of capping agents CTAB and BDAC in approximate ratio for control of nanorod length, 2.8 mL of 4 mM $AgNO_3$, 5 mL of 15 mM $HAuCL_4$, and 2.25 mL of 80 mM ascorbic acid. One hundred twenty microliters of seed solution was added to the growth solution maintained at a temperature of 28°C and allowed to equilibrate for 3 hours. The GNRs synthesized were collected using centrifugation at 10,000 rpm for 15 minutes and washed twice using deionized (DI) water to remove excess growth reagents and spherical/smaller nanoparticles. The shape, yield, and aspect ratios of the GNRs were characterized using a Philips CM10 transmission electron microscope (TEM; Philips, Amsterdam, The Netherlands) operating at 80 kV under high vacuum and room temperature. TEM grids were prepared by placing 1 μL of the nanorod solution in a 400-mesh Formvar-coated copper grid and evaporating the solution at room temperature. At least 100 to 150 nanorods were counted and measured per grid to calculate the mean aspect ratio of the nanorods after the synthesis step. The absorption spectra of the GNR samples through each stage of experiments were measured using a Spectronic 200 UV-NIR spectrophotometer (Thermo Fisher Scientific Inc.) in the wavelength range between 400 and 1000 nm.

The dimensions of the GNRs are closely related to their light scattering and absorbing capabilities. The extinction spectra of the GNRs is characterized by two peaks, the larger/dominant peak corresponding to the longitudinal surface plasmon resonance (LSPR) and the shorter peak obtained at a lower wavelength corresponding to the axial surface plasmon resonance (ASPR). The dominant LSPR peak can be tuned by carefully controlling the nanorod synthesis procedure.[34] GNRs formulations corresponding to LSPR peak of 840 nm were synthesized using the seed-mediated procedure. The plasmon peak was designed to overlap with the blue edge of the OCT imaging spectral band as shown in Figure 1, to provide a steep wavelength-dependent response.[17] TEM imaging of the GNRs corresponding to a LSPR of 840 nm, shown in Figure 1 (inset), reveals rod-shaped, well dispersed nanoparticles 45 ± 6 nm in length and 12 ± 2 nm in width.

Surface Modification of Gold Nanorods

Briefly, 1 mL of GNRs solution was diluted to 10 mL with deionized water. To this solution, 100 mL of 2 mg/mL of PAA dissolved in a 6 mM NaCl solution was added drop-wise and the resulting solution was stirred vigorously for 6 hours. At the end of the activation process the mixture was centrifuged at 15,000 rpm for 30 minutes to remove unbound molecules and the GNR pellet was then resuspended in 2 mL of MES buffer.

Anti–Glut-1 Immobilization on the Surface of Modified Gold Nanorod

Using the heretofore mentioned surface modification strategy, carboxylic groups were generated on the surface of GNRs due to the presence of PAA. Five hundred microliters of 0.1 M EDC and 500 μL of 0.1 M NHSS were added to 5 mL of modified GNRs resuspended in MES buffer (pH = 6). The GNRs were collected by centrifugation after 60 minutes of activation. The GNR pellet was then introduced into a 1 mL solution of 50 μg/mL anti–Glut-1 monoclonal antibodies and allowed to interact overnight at 4°C. The antibody bound GNRs were then separated from the excess antibody and reaction chemicals by two rounds of centrifugation at 8000 rpm for 5 minutes each. The anti–Glut-1 GNRs were then stored in 0.1% BSA in 1× PBS at 4°C. Zetapotential measurements were conducted on the GNR dispersed in DI water sample after each stage of the nanorod-antibody assembly construction. Table 1 exhibits the zetapotential measurements recorded for the anti–Glut-1 GNR construct after each step of the

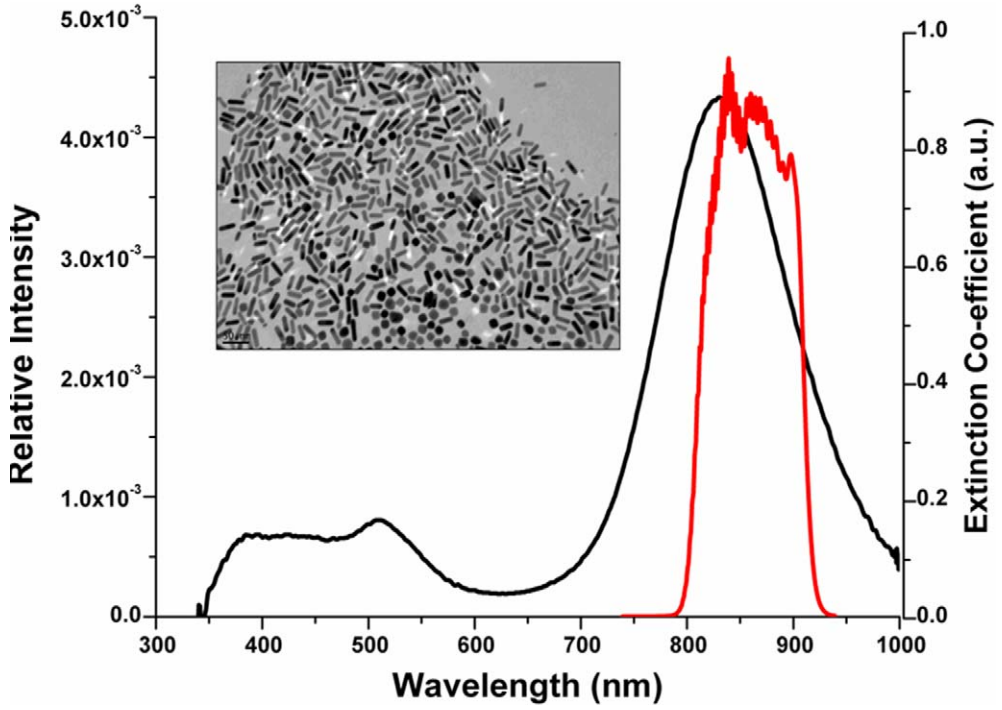

Figure 1. Extinction spectrum of GNRs (*black line*) and relative intensity of OCT imaging light (*red line*). Inset: TEM image of bare GNRs corresponding to LSPR peak of 840 nm.

Table 1. Zeta Potential Measurements of GNRs Recorded before and after Surface Modifications

Surface Activity of Nanorods (Suspended in DI Water)	Zeta Potential (ζ), mV
CTAB	38.8 ± 2
Anionic polymer (poly-acrylic acid)	−64.9 ± 5
Anti–Glut-1 labeled GNRs	−47.36 ± 3

immobilization procedure. Initially the as-produced GNRs exhibit a positive potential of 38 ± 2 mV due to presence of the stabilizing surfactant layer of CTAB. However, CTAB has been proven to be cytotoxic and does not contain any reactive groups which could be used for linking biomolecules. The coating of the GNRs with anionic polymer PAA shifts their zetapotential to –64.9 ± 5 mV. The coating of PAA on the GNRs masks the CTAB and generates reactive carboxylic groups on the surface of the GNRs. The carboxylic groups are then activated and linked to the amino groups on the surface of the antibody via a covalent bond. The attachment of the antibody to the surface of the GNRs shifts their zetapotential to –47.36 ± 3 mV. Measuring the zetapotential of the GNRs after each step enables validation that the polymer and the biomolecule have correctly attached on the surface of the GNRs.

After the antibodies were conjugated to the GNRs the construct was characterized using a modified ELISA to measure its bioactivity and binding specificity. Briefly, Glut-1 protein (positive control) and BSA (negative control) at concentrations of 0.5 μg/mL were incubated in high-binding 96-well plates at 4°C overnight. The plates were washed and then blocked with 1% BSA and 1% normal goat serum (NGS) solution in 1× PBS for 30 minutes to eliminate any nonspecific binding. The anti–Glut-1 GNR construct was then incubated in the wells for 45 minutes before rinsing the wells three times with 1× PBS and adding antirabbit IgG tagged to horseradish peroxidase (HRP). The secondary antibody was also incubated for 45 minutes and rinsed three times using 1× PBS. The peroxidase label was then developed using TMB as the calorimetric substrate as per manufacturer's protocol. The well plates were evaluated using a Fluostar Optima plate reader (BMG Labtech Inc., Cary, NC) with a white light excitation and 450 nm emission filter. Table 2 depicts the average absorbance values recorded for $n = 12$ wells for each case. Based on the absorbance values shown in Table 2 we can conclude that the anti–Glut-1-GNR constructs maintain approximately 81% of their bioactivity after conjugation to the GNRs. The anti–Glut-1-GNR constructs also do not bind to a nonspecific protein such as BSA.

Tissue Sample Selection

The specimen library of the Florida Lions Ocular Pathology Laboratory at Bascom Palmer Eye Institute was utilized to retrieve three human conjunctival tissue specimens from each of three different categories: conjunctiva without epithelial atypia (controls); conjunctival intraepithelial neoplasia, CIS; and SCC. Conjunctiva without epithelial atypia was isolated from the margins of orbital exenteration specimens or from conjunctival tissue excised from patients with a diagnosis of conjunctivochalasis. In each case, the specimen was reviewed to ensure the absence of epithelial atypia. CIS was defined as conjunctiva

Table 2. Characterization of Anti–Glut-1 Labeled GNR Bioactivity Using ELISA Plate Reader

	Empty Well	Glut-1 Protein	Glut-1 Protein	Glut-1 Protein	Glut-1 Protein	BSA	BSA
		Buffer 2′-Ab-HRP	1′-Ab 2′-Ab-HRP	Bare GNRs 2′-Ab-HRP	1′-Ab-GNRs 2′-Ab-HRP	Bare GNP 2′-Ab-HRP	1′-Ab-GNRs 2′-Ab-HRP
Average absorbance	0.595	0.619	0.885	0.623	0.719	0.552	0.535

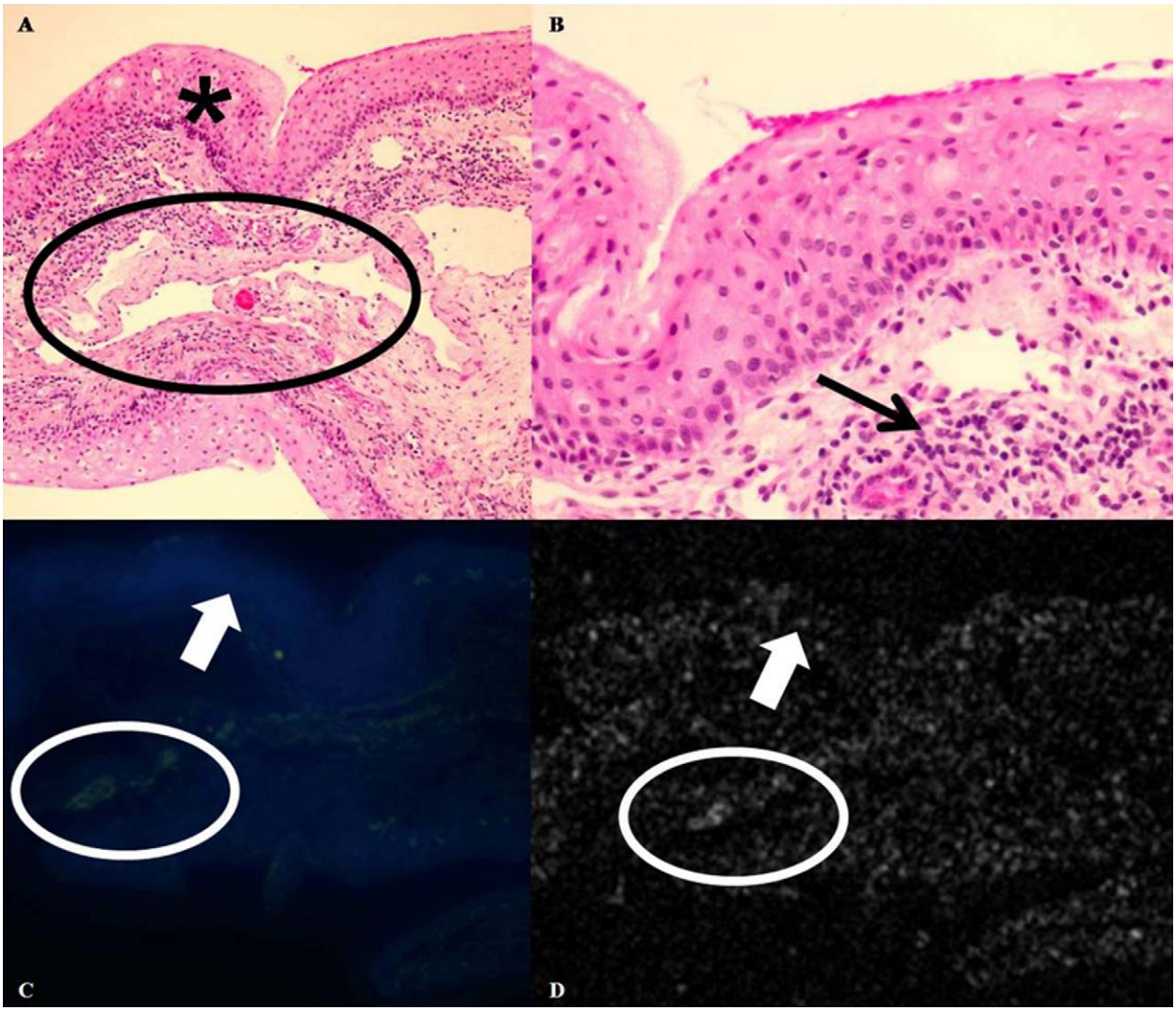

Figure 2. Normal conjunctiva control. (**A**) Photomicrograph, hemotoxylin and eosin, ×100. Conjunctival specimen with stratified, nonkeratinized mucosal epithelium (*asterisk*). Scattered capillaries and dilated lymphatic channels are present within the substantia propria (*black oval*). (**B**) Photomicrograph, hemotoxylin and eosin, ×400. No faulty epithelial maturational sequencing or cellular atypia is present within the epithelium. A mild chronic inflammatory cell infiltrate is present within the substantia propria (*black arrow*). (**C**) Immunofluorescence, ×50. DAPI stains cell nuclei of epithelial cells in *blue*. No green immunofluorescent staining is present within the epithelium, indicating lack of binding of functionalized GNRs to the normal epithelial cells (*white arrow*). A mild amount of green immunofluorescence is present within the substantia propria (**C**) (*white oval*) in a location correlating to that of scattered capillaries seen in (**A**) (*black oval*), indicating binding of the functionalized GNRs to erythrocytes. (**D**) OCT. The same portion of tissue seen in (**C**) is imaged using OCT. A faint background signal without conspicuous areas of increased signal scattering is observed within the epithelium (*white arrow*), indicating lack of functionalized GNRs in this area. A trace increase in signal scattering is present within the substantia propria (*white oval*) in an area correlating to location of both immunofluorescent staining in (**C**) and capillaries in (**A**).

displaying faulty epithelial maturational sequencing, with cellular atypia and loss of the normal polarity of the epithelium extending to the full thickness of the epithelium, but with an intact epithelial basement membrane and no invasion of the atypical epithelial cells into the underlying substantia propria. SCC was defined as conjunctiva displaying faulty epithelial maturational sequencing extending to full thickness, with definite invasion of the atypical epithelium into the underlying substantia propria.

Tissue Processing

Paraffin embedded tissues were cut into 5 micron slices and placed on glass slides. The slides were incubated at 37°C overnight to melt the paraffin. The tissue samples were dewaxed using sequential baths of xylene (10 minutes), and decreasing ethanol solutions consisting of two baths of absolute, two baths of 95%, one bath of 90% for one minute each. The slides were then placed in Tris Buffer Saline (S1968; DAKO, Glostrup, Denmark) bath for 1 minute. Antigen retrieval was done by incubating slides for 20 minutes in target retrieval solution (20 mL target retrieval [DAKO S1699; DAKO] + 180 mL DH_2O), heated to 90°C. The slides were then cooled in the same container for 20 minutes. Permeabilization of tissue was performed by incubating slides for 5 minutes in 0.1% Triton-100 solution. Nonspecific binding was blocked by incubation of slides in 1% BSA and 1% NGS in 1× PBS for 1 hour. Two hundred microliters of polyclonal anti–Glut-1 antibody (Thermo Fisher Scientific Inc.) labeled GNRs were incubated with each slide for 1 hour in a humidity chamber. The slides were washed using 1× PBS solutions for 5 minutes in three baths. Slides were then incubated with Alexa-488 (Fluorophore) labeled antirabbit IgG (Secondary Antibody) (Invitrogen Inc.) at a concentration of 1:500

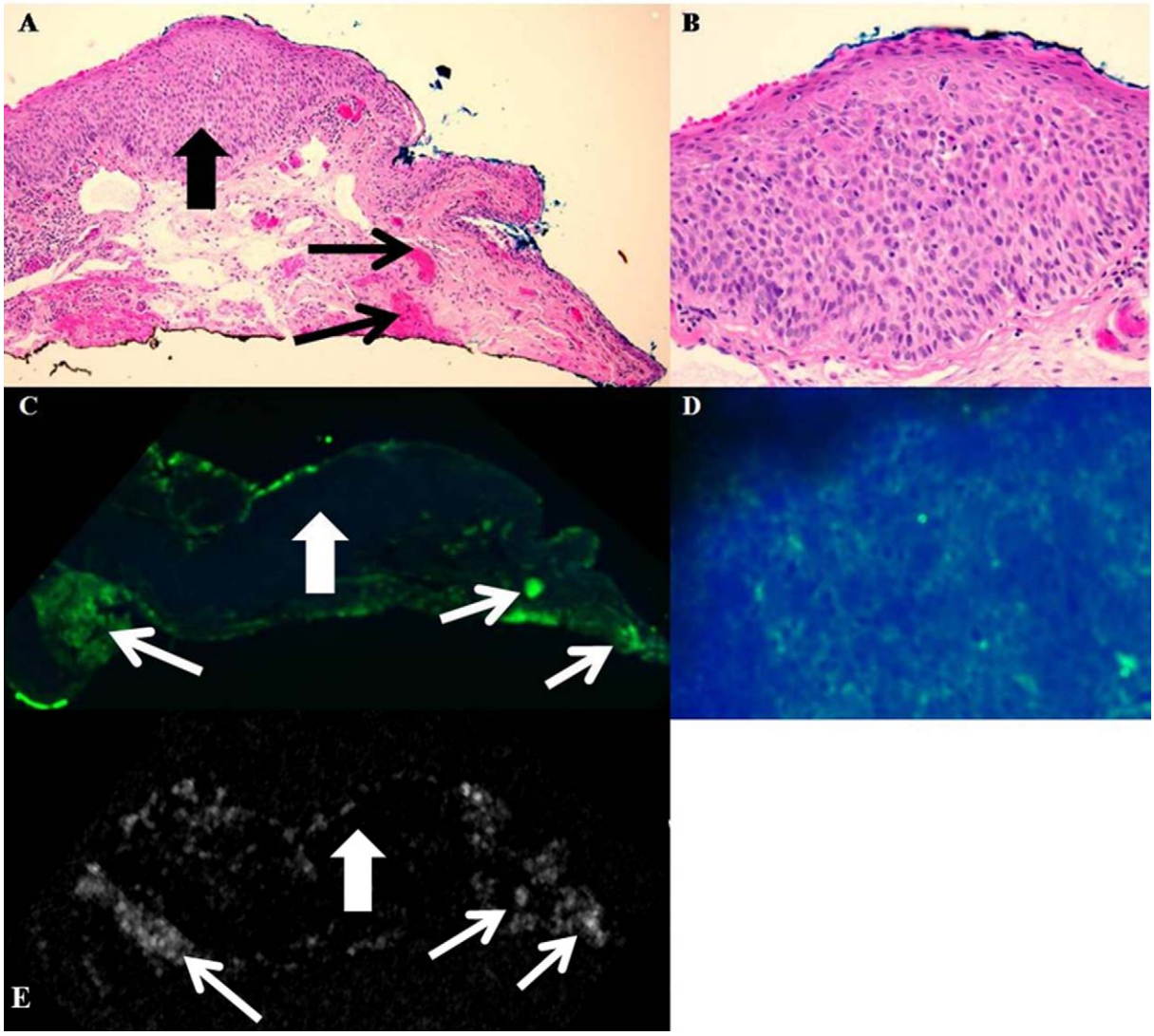

Figure 3. Conjunctival intraepithelial neoplasia: carcinoma in situ. (**A**) Photomicrograph, hemotoxylin and eosin, ×100. Conjunctival specimen displays faulty epithelial maturational sequencing extending to full thickness (*large black arrow*). The epithelial basement membrane is intact, and no invasion into the underlying substantia propria is present. Foci of capillaries and hemorrhage are present in the substantia propria (*small black arrows*). (**B**) Photomicrograph, hemotoxylin and eosin, ×400. The epithelium displays faulty epithelial maturational sequencing, with cellular atypia and loss of the normal epithelial polarity extending to full thickness. (**C**) Immunofluorescence, ×50. The epithelium displays faint green staining due to fluorescent tagged secondary antibody, indicating binding of functionalized GNRs to atypical epithelial cells (*large white arrow*). Intense staining is observed in areas correlating to foci of capillaries and hemorrhage within the substantia propria (*small white arrows*). (**D**) Immunofluorescence, ×400. High magnification immunofluorescence discloses green fluorescent staining of atypical epithelium in a membranous staining pattern, indicating presence of functionalized GNRs bound to atypical epithelial cells, which are overexpressing Glut-1. (**E**) OCT. No increase in signal scattering was observed within the epithelium (*large white arrow*), while multiple foci of increased signal scatter correlating to areas of hemorrhage were present within the substantia propria (*small white arrows*).

diluted in 0.1% BSA and 0.1% NGS in 1× PBS for a period of 1 hour. The slides were washed using 1× PBS solutions for 5 minutes in three baths. Nuclei of tissue were stained with 1:1000 concentration of 4′,6-diamidino-2-phenylindole (DAPI) in 1× PBS for 5 minutes. Slides were washed using 1× PBS solutions for 5 minutes in three baths. Fluorescence imaging of the tissue was done using Axio Imager 2 from Carl Zeiss (Oberkochen, Germany) using the 5× and 40× lenses. OCT imaging was then performed using the Bioptigen (Durham, NC) SD-OCT. The telecentric lens was used with a rastor scanning protocol covering a rectangular area of 3 × 3 mm. Every imaging session consisted of 275 A scan and 275 B scan, with an imaging depth of 2 μm. The slides were always positioned at a 45° angle during OCT imaging to reduce the amount of noise observed due to the reflected light measured by the detector. The reported resolution of the OCT system for a small animal eye is 3.3 μm. Image processing that included image averaging and background subtraction for noise cancellation was conducted using Matlab (Mathworks, Natick, MA).

Results

Tissue Staining and Imaging Using OCT

Light microscopic review of the three normal conjunctival controls confirmed the absence of epithelial atypia (Figs. 2A, 2B). Following incubation of the tissue with anti–Glut-1 conjugated GNRs and application of fluorescent tagged secondary antibodies, immunofluorescence imaging disclosed no binding of the functionalized GNRs to the epithelium in any of the three normal controls (Fig. 2C). A mild amount of

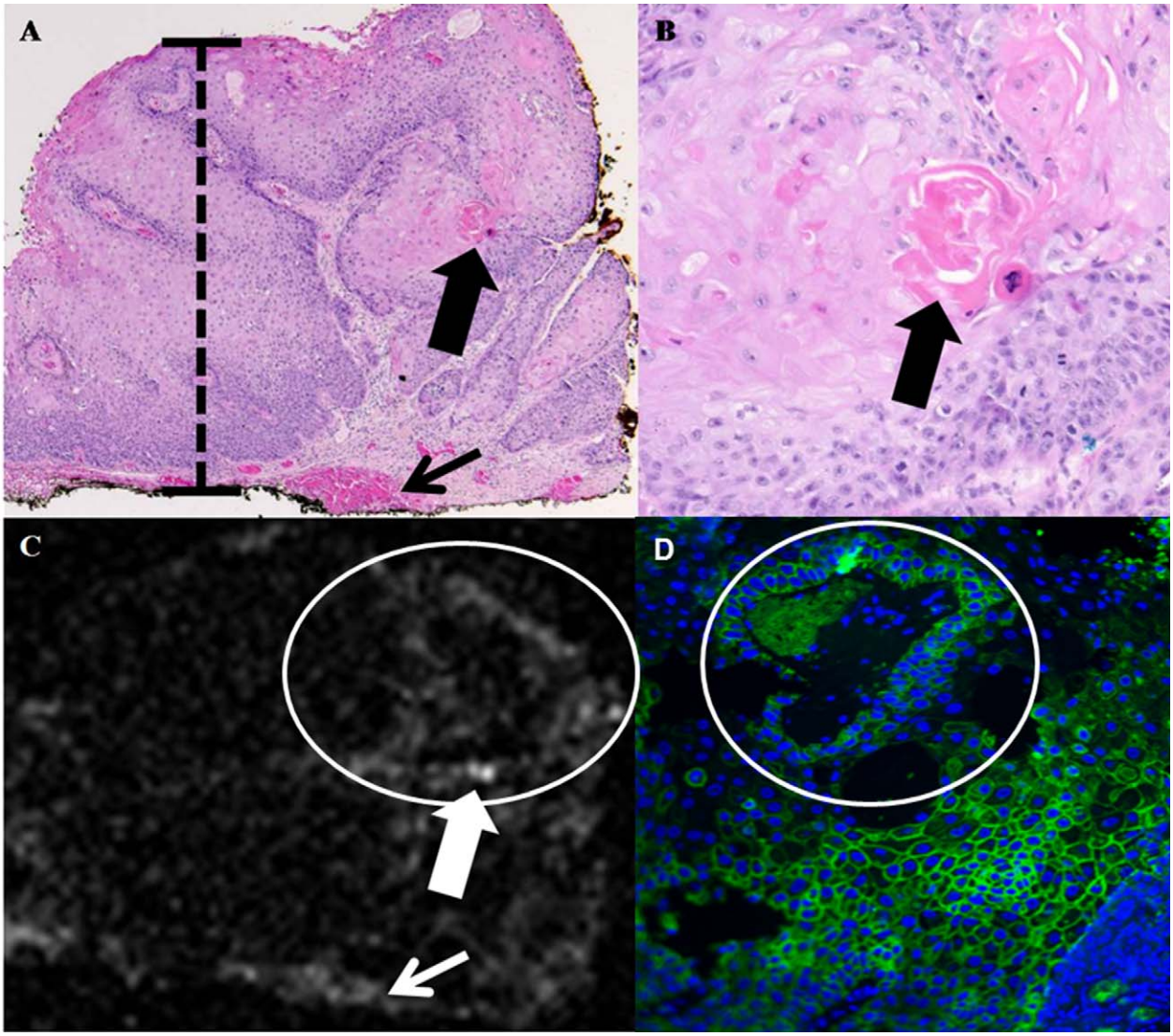

Figure 4. Conjunctival squamous cell carcinoma. (**A**) Photomicrograph, hemotoxylin and eosin, ×40. The conjunctival epithelium displays faulty epithelial maturation sequencing extending to full thickness (*black bar*). Invasion of atypical epithelial cells with foci of dyskeratosis is present (*large black arrow*). A focus of hemorrhage is present at the deep margin of the specimen (*small black arrow*). (**B**) Photomicrograph, hemotoxylin and eosin, ×400. Higher magnification view of area denoted by *large black arrow* in (**A**) discloses formation of a keratin pearl by atypical epithelial cells within the substantia propria. (**C**) OCT. Area of atypical tumor cells depicted in (**B**) is detectable as a focus of increased OCT signal scattering (*large white arrow*) in (**C**). Focus of hemorrhage depicted in (**A**) is also visible as an increase in OCT signal scatter (*small white arrow*) in (**C**). (**D**) Immunofluourescence, ×400. Atypical epithelial cells surrounding the keratin pearl depicted in (**B**) and visible as increased signal scatter in (**C**) stained intensely positive on immunofluorescence, indicating a high level of overexpresion of Glut-1 and strong binding by functionalized GNRs.

fluorescent staining was observed within the subepithelial tissue (substantia propria) in areas correlating to the location of capillaries and foci of hemorrhage present within each of the three controls (Fig. 2C). This positive staining indicates binding of the functionalized GNRs to erythrocytes. OCT images of each control specimen disclosed a faint tissue background signal within the epithelium, which was without conspicuous areas of increased signal scattering (Fig. 2D). The signal intensity within the epithelium of tissue treated with functionalized GNRs correlated to that observed on OCT images of tissue treated with nonfunctionalized GNRs and washed (OCT control images) in all cases. In all three control specimens, trace areas of increased OCT signal scattering were observed within the substantia propria that correlated to foci of positive staining observed on immunofluorescence, indicating binding of the functionalized GNRs to erythrocytes was detectable as an increase in signal scattering on OCT (Fig. 2D).

Histopathologic review of three conjunctival specimens with a diagnosis of conjunctival intraepithelial neoplasia: carcinoma in situ confirmed the presence of epithelium which displayed faulty epithelial maturation sequencing extending to full thickness, without invasion into the underlying substantia propria (Figs. 3A, 3B). Immunofluorescence disclosed moderately intense staining of atypical epithelial cells in a membranous staining pattern in all three CIS specimens, indicating binding of functionalized GNRs to atypical cells overexpressing the Glut-1 protein (Figs. 3C, 3D). As in the three normal conjunctiva controls, intense staining correlating to foci of capillaries and hemorrhage was present in each specimen, indicating strong binding of functionalized GNRs to erythrocytes (Fig. 3C). On OCT, a faint background signal without conspicuous areas of increased signal scattering was observed within the epithelium, while in the substantia propria, each specimen displayed discrete areas of increased signal scatter

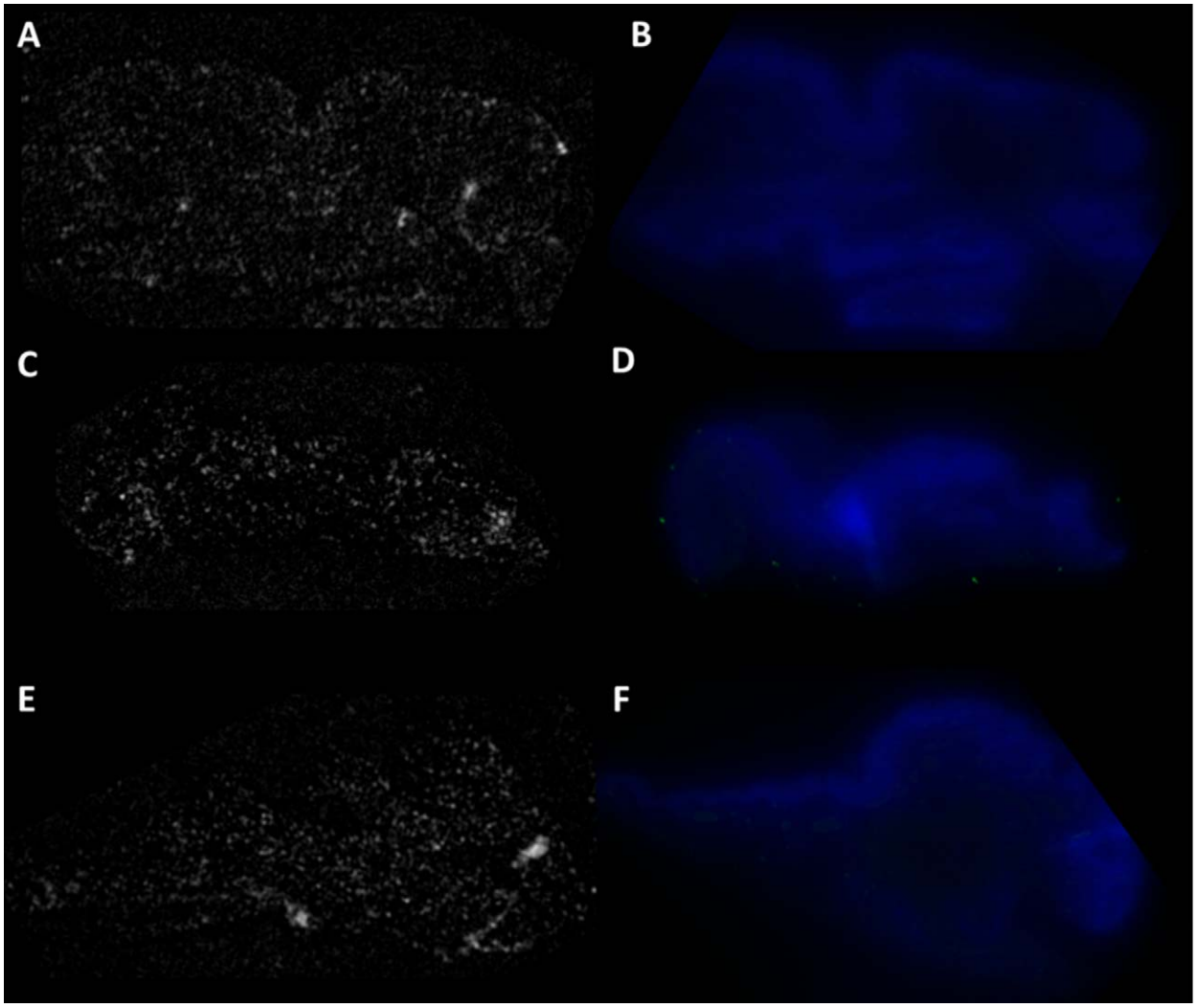

Figure 5. OCT images: (**A**) normal conjunctiva, (**C**) conjunctival intraepithelial neoplasia: carcinoma in situ (**E**) conjunctival squamous cell carcinoma. No regions of enhanced scattering were observed, which rules out any nonspecific binding of PAA coated GNRs to tissue. Fluorescence imaging: (**B**) normal conjunctiva, (**D**) conjunctival intraepithelial neoplasia: carcinoma in situ (**F**) conjunctival squamous cell carcinoma. DAPI stains cell nuclei of epithelial cells in *blue*. No areas of green fluorescence were observed, which rules out the nonspecific binding of Alexa-488 tagged secondary antibody to the tissue surface.

within the substantia propria correlating to areas of hemorrhage seen on both immunofluorescence and hemotoxylin and eosin stained sections (Fig. 3E).

Histopathologic review of three specimens with a diagnosis of conjunctival squamous cell carcinoma confirmed the presence of faulty epithelial maturation sequencing extending to full thickness, with invasion of atypical epithelial cells into the underlying substantia propria (Figs. 4A, 4B). In these three specimens, a moderate (one case) to marked (two cases) amount of staining was observed via immunofluorescence in the atypical epithelial cells, indicating overexpression of Glut-1 and binding to these cells by the functionalized GNRs (Fig. 4D). As in all previous cases, foci of capillaries and hemorrhage within the tissue where intensely positive. On OCT, foci of increased signal scattering corresponding to areas of intensely immunofluorescence-positive, atypical epithelial cells were present in two of three cases (Fig. 4C). No enhancement of OCT signal scattering was present in one case despite the observation of a moderate amount of intraepithelial staining via immunofluorescence. As in the previous cases, foci of increased OCT signal scattering corresponding to areas of hemorrhage and capillaries were present in each specimen (Fig. 4C).

To confirm that the fluorescence and OCT signal originate from the binding of anti–Glut-GNR construct to the Glut-1 protein expressed by tissue and rule out nonspecific binding, we incubated tissue specimens from each case initially with nonspecific and nontargeted, PAA-coated GNRs and then with secondary fluorescent tagged antibody. Figure 5 shows the fluorescence and OCT images recorded for the three control tissue specimens tested. OCT images shown in Figures 5A, 5C, and 5E show no regions of enhanced scattering. Therefore, we can conclude that PAA-coated GNRs do not bind nonspecifically to tissue. Fluorescence images shown in Figures 5B, 5D, and 5F do not show any regions of green fluorescence, which would correlate to the binding of Alexa-488 labeled secondary antibodies on tissue.

Discussion

No binding of our functionalized contrast agent was observed within the epithelium of the three normal conjunctiva

controls. This was expected, given we did not anticipate Glut-1 overexpression within morphologically normal epithelium. In the six total cases of OSSN tested, immunofluorescence disclosed variable-intensity binding of the functionalized contrast agent, suggesting interlesional variability with regards to degree of Glut-1 overexpression. In two of three cases of SCC, binding of the atypical epithelial cells by the functionalized contrast agent was sufficient to produce an increased scattering effect on OCT, which correlated to areas of intense staining observed on immunofluorescence. This result suggests a "threshold" amount of GNRs is required within the tissue to produce an observable increase in signal scattering. Given the fact that increased OCT signal scattering was observed within areas correlating to foci of capillaries and hemorrhages in all nine tested specimens, the level of expression of Glut-1 by erythrocytes, and by extension, the concentration of functionalized GNRs present in those areas may serve as a useful proxy to determine the threshold amount of GNRs which must be present within a tissue specimen to produce increased OCT scattering. It appears that in OSSN, only the most severely dysplastic lesions (SCC) exhibit a level of Glut-1 overexpression necessary to pass the threshold required by our technique.

Our study has a number of important limitations. The image quality of the OCT images was likely hampered by the use of formalin fixed, deparaffinized, rehydrated tissue samples. Future work will focus on overcoming this limitation by improving imaging processing, possibly utilizing ultra high resolution OCT systems, and ultimately by transitioning to in vivo studies using animal models, where the issue of tissue quality can be avoided.

While the choice of OSSN as a model tissue analyte provided ample tissue specimens and a spectrum of disease severity with which to challenge our imaging technique, the choice of Glut-1 as a molecular marker was problematic. Unfortunately, we know of no other marker commonly employed in the evaluation of OSSN, the diagnosis of which is typically made on the basis of morphology. Additional work involving other ocular surface lesions with additional molecular markers is underway. The lack of specificity of Glut-1 posed an additional challenge. While the intense binding of our functionalized GNRs to erythrocytes consistently produced a detectable increase in OCT signal scattering that was helpful in demonstrating proof of concept, future work will focus on the utilization of lesion-specific markers to avoid nonspecific binding. Finally, the interlesional variability in Glut-1 expression and the membranous staining pattern likely contributed to the inability to visualize three CIS lesions and one SCC lesion on OCT. Identification of markers with consistently high levels of expression in a nuclear or cytoplasmic location may increase the sensitivity of our technique.

In spite of these limitations, there are several advantages of using GNRs as contrast agents for OCT imaging. GNRs are bio-inert and biocompatible[35] and have been successfully used in animal eyes for contrast enhanced photoacoustic imaging,[36] drug/gene delivery,[37,38] and anti-angiogenic properties.[39] GNRs in conjunction with OCT can be used to highlight areas overexpressing certain biomarkers. This model can be utilized for monitoring specific disease loads by conjugating an appropriate targeting molecule to the GNR, allowing the diagnosis and monitoring of disease on a molecular level, which cannot be accomplished using high resolution, noncontrast OCT systems. Noncontrast OCT systems can provide high definition structural information of tissue; however, they do not provide any biochemical and molecular information.

Conclusions

We have demonstrated the successful use of a commercially available OCT system toward molecular histopathology utilizing functionalized GNRs as molecular markers to image ocular tissue in the setting of OSSN. Future work will focus on refinement of image quality, identification of ideal molecular markers, and transitioning to in vivo studies, with the ultimate goal of expanding the diagnostic capabilities of OCT by achieving noninvasive, in vivo optical biopsy with molecular specificity.

References

1. Huang D, Swanson EA, Lin CP, et al. Optical coherence tomography. *Science*. 1991;254:1178–1181.
2. Ko TH, Fujimoto JG, Schuman JS, et al. Comparison of ultrahigh- and standard-resolution optical coherence tomography for imaging macular pathology. *Ophthalmology*. 2005; 112:1922.e1–15.
3. Drexler W, Morgner U, Kärtner FX, et al. In vivo ultrahigh-resolution optical coherence tomography. *Opt Lett*. 1999;24: 1221–1223.
4. Drexler W. Ultrahigh-resolution optical coherence tomography. *J Biomed Opt*. 2004;9:47–74.
5. Fujimoto JG. Optical coherence tomography for ultrahigh resolution in vivo imaging. *Nat Biotechnol*. 2003;21:1361–1367.
6. Boppart SA, Oldenburg AL, Xu C, et al. Optical probes and techniques for molecular contrast enhancement in coherence imaging. *J Biomed Opt*. 2005;10:041208.
7. Oldenburg AL, Hansen MN, Zweifel DA, et al. Plasmon-resonant gold nanorods as low backscattering albedo contrast agents for optical coherence tomography. *Opt Express*. 2006; 14:6724–6738.
8. Sirotkina M, Shirmanova M, Bugrova M, et al. Continuous optical coherence tomography monitoring of nanoparticles accumulation in biological tissues. *J Nanopart Res*. 2011;13: 283–291.
9. Liao H, Nehl CL, Hafner JH. Biomedical applications of plasmon resonant metal nanoparticles. *Nanomedicine*. 2006; 1:201–208.
10. Kim CS, Wilder-Smith P, Ahn YC, et al. Enhanced detection of early-stage oral cancer in vivo by optical coherence tomography using multimodal delivery of gold nanoparticles. *J Biomed Opt*. 2009;14:034008.
11. Huang X, Neretina S, El-Sayed MA. Gold nanorods: from synthesis and properties to biological and biomedical applications. *Adv Mater*. 2009;21:4880–4910.
12. Tong L, Wei Q, Wei A, et al. Gold nanorods as contrast agents for biological imaging: optical properties, surface conjugation and photothermal effects. *Photochem Photobiol*. 2009;85:21–32.
13. Aizpurua J, Bryant GW, Richter LJ, et al. Optical properties of coupled metallic nanorods for field-enhanced spectroscopy. *Physical Review B*. 2005;71:235420.
14. Troutman TS, Barton JK, Romanowski M. Optical coherence tomography with plasmon resonant nanorods of gold. *Opt Lett*. 2007;32:1438–1440.
15. Alekseeva A, Bogatyrev V, Khlebtsov B, et al. Gold nanorods: synthesis and optical properties. *Colloid J*. 2006;68:661–678.
16. Sönnichsen C, Franzl T, Wilk T, et al. Drastic reduction of plasmon damping in gold nanorods. *Phys Rev Lett*. 2002;88: 77402.
17. Oldenburg AL, Hansen MN, Ralston TS, et al. Imaging gold nanorods in excised human breast carcinoma by spectroscop-

ic optical coherence tomography. *J Mater Chem*. 2009;19: 6407–6411.

18. Lee GA, Hirst LW. Ocular surface squamous neoplasia. *Surv Ophthalmol*. 1995;39:429–450.
19. Gurses I, Doganay S, Mizrak B. Expression of glucose transporter protein-1 (Glut-1) in ocular surface squamous neoplasia. *Cornea*. 2007;26:826–830.
20. Gould GW, Holman G. The glucose transporter family: structure, function and tissue-specific expression. *Biochem J*. 1993;295:329–341.
21. Gerhart DZ, Levasseur RJ, Broderius MA, et al. Glucose transporter localization in brain using light and electron immunocytochemistry. *J Neurosci Res*. 1989;22:464–472.
22. Yamamoto T, Seino Y, Fukumoto H, et al. Over-expression of facilitative glucose transporter genes in human cancer. *Biochem Biophys Res Commun*. 1990;170:223–230.
23. Younes M, Lechago LV, Somoano JR, et al. Wide expression of the human erythrocyte glucose transporter Glut1 in human cancers. *Cancer Res*. 1996;56:1164–1167.
24. Carvalho KC, Cunha IW, Rocha RM, et al. GLUT1 expression in malignant tumors and its use as an immunodiagnostic marker. *Clinics*. 2011;66:965–972.
25. Macheda ML, Rogers S, Best JD. Molecular and cellular regulation of glucose transporter (GLUT) proteins in cancer. *J Cell Physiol*. 2005;202:654–662.
26. Zu XL, Guppy M. Cancer metabolism: facts, fantasy, and fiction. *Biochem Biophys Res Commun*. 2004;313:459–465.
27. Gelender H, Forster R. Papanicolaou cytology in the diagnosis and management of external ocular tumors. *Arch Ophthalmol*. 1980;98:909–912.
28. Tseng S. Staging of conjunctival squamous metaplasia by impression cytology. *Ophthalmology*. 1985;92:728–733.
29. Tsubota K, Kajiwara K, Ugajin S, et al. Conjunctival brush cytology. *Acta Cytol*. 1990;34:233–235.
30. Duchateau N, Hugol D, d'Hermies F, et al. Contribution of in vivo confocal microscopy to limbal tumor evaluation [in French]. *J Fr Ophtalmol*. 2005;28:810–816.
31. Malandrini A, Martone G, Traversi C, et al. In vivo confocal microscopy in a patient with recurrent conjunctival intraepithelial neoplasia. *Acta Ophthalmol (Copenh)*. 2008;86:690–691.
32. Kieval JZ, Karp CL, Shousha MA, et al. Ultra-high resolution optical coherence tomography for differentiation of ocular surface squamous neoplasia and pterygia. *Ophthalmology*. 2011;119:481–486.
33. Vajzovic LM, Karp CL, Haft P, et al. Ultra high-resolution anterior segment optical coherence tomography in the evaluation of anterior corneal dystrophies and degenerations. *Ophthalmology*. 2011;118:1291–1296.
34. Murphy CJ, Thompson LB, Chernak DJ, et al. Gold nanorod crystal growth: from seed-mediated synthesis to nanoscale sculpting. *Curr Opin Colloid Interface Sci*. 2011;16:128–134.
35. Bakri SJ, Pulido JS, Mukherjee P, et al. Absence of histologic retinal toxicity of intravitreal nanogold in a rabbit model. *Retina*. 2008;28:147–149.
36. Li PC, Wang CRC, Shieh DB, et al. In vivo photoacoustic molecular imaging with simultaneous multiple selective targeting using antibody-conjugated gold nanorods. *Opt Express*. 2008;16:18605–18615.
37. Hayashi A, Naseri A, Pennesi ME, et al. Subretinal delivery of immunoglobulin G with gold nanoparticles in the rabbit eye. *Jpn J Ophthalmol*. 2009;53:249–256.
38. Singh S, Grossniklaus H, Kang S, et al. Intravenous transferrin, RGD peptide and dual-targeted nanoparticles enhance anti-VEGF intraceptor gene delivery to laser-induced CNV. *Gene Ther*. 2009;16:645–659.
39. Mukherjee P, Bhattacharya R, Wang P, et al. Antiangiogenic properties of gold nanoparticles. *Clin Cancer Res*. 2005;11: 3530–3534.